Pol. J. Environ. Stud. Vol. XX, No. X (XXXX), 1-15
DOI: *10.15244/pjoes/224835* ONLINE PUBLICATION DATE: 2026-09-04

Original Research

Experimental Study Online Detection of Toluene Secondary Organic Aerosol by Synchrotron Radiation Vacuum Ultraviolet Photoionization Mass Spectrometer

Mincong Zhu[1], Mingqiang Huang[1]*, Xiaobin Shan[2], Liusi Sheng[2], Xingqiang Liu[3], Weixiong Zhao[4], Xuejun Gu[4], Weijun Zhang[4]**

[1]Fujian Provincial Key Laboratory of Modern Analytical Science and Separation Technology, College of Chemistry & Chemical Engineering and Environment, Minnan Normal University, Zhangzhou 363000, China
[2]National Synchrotron Radiation Laboratory, University of Science and Technology of China, Hefei 230031, China
[3]School of Environment Science & Engineering, Tan Kah Kee College, Xiamen University, Zhangzhou 363105, China
[4]Laboratory of Atmospheric Physico-Chemistry, Anhui Institute of Optics and Fine Mechanics, Chinese Academy of Sciences, Hefei 230031, China

Received: 23 March 2026
Accepted: 19 June 2026

Abstract

Secondary organic aerosols (SOAs) formed via the photooxidation of toluene and other aromatics are major components of fine particles. A synchrotron radiation vacuum ultraviolet photoionization aerosol mass spectrometer (VUV-PIAMS) was used to conduct online detection of the components of SOA generated by toluene chamber simulation in this study. Mass spectra of SOA particles were measured at a photon energy of 10.5 eV. The photoionization efficiency (PIE) curve of each ion peak within the 7.5-11.5 eV range was obtained, and then the qualitative analysis based on ionization potential (IP) was utilized to determine the composition of SOA. Experimental results demonstrated that mass spectra of toluene SOA primarily contained peaks at m/z = 64, 72, 94, 106, 108, and 122, with IPs of 8.92±0.03, 9.63±0.03, 8.53±0.03, 9.45±0.03, 8.28±0.03, 8.93±0.03, and 9.26±0.03 eV, respectively. Combined with theoretical calculations and offline measurements of ultraviolet-visible absorption spectroscopy and electrospray ionization mass spectrometry, it was determined that furan, methylglyoxal, phenol, benzaldehyde, 2-methylphenol, 4-methylphenol, and benzoic acid were the major components of toluene SOA. Based on the areas of the mass peaks, methylphenol, benzaldehyde, benzoic acid, methylglyoxal, phenol, furan, and unidentified components accounted for 21.4%, 17.1%, 15.7%, 14.3%, 12.9%, 11.4% and 7.2% of the measured components, respectively. The obtained results provide new information for studying the photooxidation mechanism of toluene. VUV-PIAMS overcomes cumbersome sample preparation procedures, potential secondary contamination, and other shortcomings of offline

*e-mail: huangmingqiang@mnnu.edu.cn
**e-mail: wjzhangaiofm@gmail.com
Tel.: +86-596-2591445
Fax: +86-596-2591337
0000-0003-0969-0565

measurements, making it a useful tool for measuring the compositions of SOA and revealing their formation processes.

Keywords: toluene, secondary organic aerosol, synchrotron radiation, photoionization, reaction mechanism

Introduction

Benzene, toluene, and other aromatic hydrocarbon compounds emitted from sources like vehicle exhaust, industrial production, and the use of solvents such as paints and adhesives are typical representatives of anthropogenic atmospheric pollutants [1, 2]. Benzene, toluene, ethylbenzene, and xylene (BTEX) account for approximately 60-75% of atmospheric aromatic compounds [3, 4]. Toluene is the most abundant aromatic hydrocarbon and also a common harmful environmental pollutant in the atmosphere. It has certain toxicity itself, can reduce the function of the central nervous system, cause hormonal imbalance between men and women, slow and abnormal fetal development, and has potential impacts on fertility [5, 6]. In addition, toluene emitted into the atmosphere mainly undergoes photooxidation reactions with OH radicals to generate secondary organic aerosol (SOA) [7-9], which can diminish atmospheric visibility [10, 11] and pose a threat to human health [12, 13]. The research on its chemical composition and formation process has attracted widespread attention.

The atmospheric photooxidation process of toluene with OH radicals has often been experimentally simulated in a smog chamber. SOA was collected with filters or impactors, extracted with organic solvents, and then detected offline by gas (or liquid) chromatography-mass spectrometry, infrared spectroscopy, etc. [7-9, 14]. Also, aerosol mass spectrometers with ionization sources such as electron bombardment and laser desorption ionization were utilized to detect the components of SOA online [15-17]. But the above methods had certain limitations. Offline methods required cumbersome sample preparation procedures and might cause secondary contamination, while aerosol mass spectrometers produced a large amount of fragment ions during measurement. For the complex products generated by toluene photooxidation, the obtained mass spectra of SOA mainly consisted of fragment ion peaks [14, 18]. Thus, "soft ionization" is extremely necessary for the measurement of chemical components of SOA [18].

Synchrotron radiation is the electromagnetic radiation emitted tangentially by charged particles moving at near-light speeds during curved motion, characterized by high intensity, broad spectral range, and excellent collimation [19]. With its high photon density, synchrotron radiation in the vacuum-ultraviolet (VUV) region serves as a photoionization source capable of achieving single-photon ionization [19-21]. A synchrotron radiation VUV photoionization aerosol mass spectrometer (VUV-PIAMS) can be utilized for the detection of aerosols in real-time. VUV-PIAMS employs aerodynamic lenses to focus aerosol particles, which undergo adiabatic sonic expansion to generate a collimated particle beam. This beam strikes the heated metal plate, causing the components of the aerosol particles to volatilize into gas and enter the ionization chamber, where the gas is ionized after crossing the VUV synchrotron radiation beam perpendicularly. The generated ions are detected using a reflection time-of-flight mass spectrometer, and the chemical composition of particles is determined by analyzing the mass spectra [20, 22-24].

VUV ionization is a single-photon ionization technique. When the energy of the photon is higher than the ionization potential of the sample molecule, the molecule can absorb the energy of a single photon and lose an electron to obtain the molecular ion, which basically achieves "soft ionization" [19-21]. Therefore, the mass spectra obtained by VUV-PIAMS measurements primarily consist of molecular ion peaks of the sample molecules. In addition, by scanning the wavelength of synchrotron radiation, a photoionization efficiency (PIE) curve for each peak was obtained, and molecular structural information of the tested sample was determined from the ionization potential [20-24]. Thus, a smog chamber and VUV-PIAMS were combined to online measure the chemical components of SOA particles generated by the photooxidation of toluene in this study. The verification was carried out by combining quantum chemical calculations and offline measurements of ultraviolet-visible absorption spectroscopy and electrospray ionization mass spectrometry. Based on the measured component information, the photooxidation mechanism of toluene was explored, which provides a basis for investigating the chemical processes of toluene and other aromatic hydrocarbons in the atmosphere.

Materials and Methods

Materials

Toluene (>99%), hydrogen peroxide (30%), and methanol (>99%) were provided by Aladdin Reagent (Shanghai) Co., Ltd. Argon (>99.9%) was purchased from Nanjing Special Gas Factory Co., Ltd.

Online Detection of Toluene Fine Particles

Referring to our previous experimental method [17], 0.1 mol/L toluene solution was prepared (toluene was dissolved in 2% methanol water solution) and atomized

with an Aerosol Generator (TSI 9302, TSI Corporation, USA) to generate aerosol particles, which passed through the silica gel drying tube to form toluene fine particles with a size in the range of 0.1-2 μm and the concentration of approximately 200 μg/m^3. The online measurement of toluene fine particles was performed with VUV-PIAMS at Hefei National Synchrotron Radiation Laboratory. As shown in Fig. 1, fine particles were focused into a collimated particle beam via an aerodynamic lens. The particle beam then collided with the heated metal plate (180ºC) to volatilize and form gas, which then entered the ionization chamber and was ionized by synchrotron radiation. The formed ions were detected by a reflection time-of-flight mass spectrometer. The mass spectra of toluene were measured by adjusting the photon energy of the synchrotron radiation to 10.5, 13.0, and 15.5 eV, respectively. During the experiment, the filtered argon gas pressure was 436 Pa, the beam source chamber (SC) pressure was greater than 10^{-1} Pa, the vacuum in the ionization chamber was maintained at 1.3×10^{-4} Pa, and the mass spectrometry sampling time was 100 s. The monochromator was scanned with a step size of 0.03 eV over the 7.5-11.5 eV range, and the obtained signal was normalized using a silicon photodiode to acquire a photoionization efficiency (PIE) curve [22, 24, 25]. Benefiting from the high photon flux and stable soft ionization characteristics of the synchrotron radiation vacuum ultraviolet light source, the VUV-PIAMS system exhibited superior anti-interference performance. The signal-to-noise ratio (SNR) of stable molecular ion peaks of detected products was 50-200.

Formation and Online Detection of Toluene SOA

Experiments were performed in a home-made chamber device. As displayed in Fig. 1, this device was mainly composed of an injection system, a Teflon chamber, and a detection system. The injection system was composed of a clean air generation device, a gas distribution platform, etc., to prepare the gas of the required concentration for the experiment in the Teflon chamber. The Teflon chamber was made of FEP-Teflon material with a thickness of 75 μm. It was approximately cylindrical in shape, with a volume of 850 L and a surface area to volume ratio of 6.5 m^{-1}. Twelve ultraviolet lamps (with radiation wavelengths of 300-400 nm) were installed around the Teflon chamber. The detection system was equipped with an HMT 333 sensor (Vaisala, Finland), gas chromatography with flame ionization detector (GC-FID, 7820A, Agilent Technologies, USA, SNR greater than 100), scanning mobility particle size analyzer (SMPS, 3080L DMA, 3775 CPC, TSI Corporation, USA, stable SNR above 100) and other instruments to measure the temperature, humidity, gas and particulate matter concentrations in the Teflon chamber [16, 25, 26]. Before each experiment, SMPS and GC-FID were calibrated according to the method provided in the Supplementary Information.

Each experiment was carried out in triplicate, with relative humidity and temperature regulated at 37±3% and 25±1ºC. Similar to our previous experiments [16, 25, 26], after cleaning the Teflon chamber, about one-

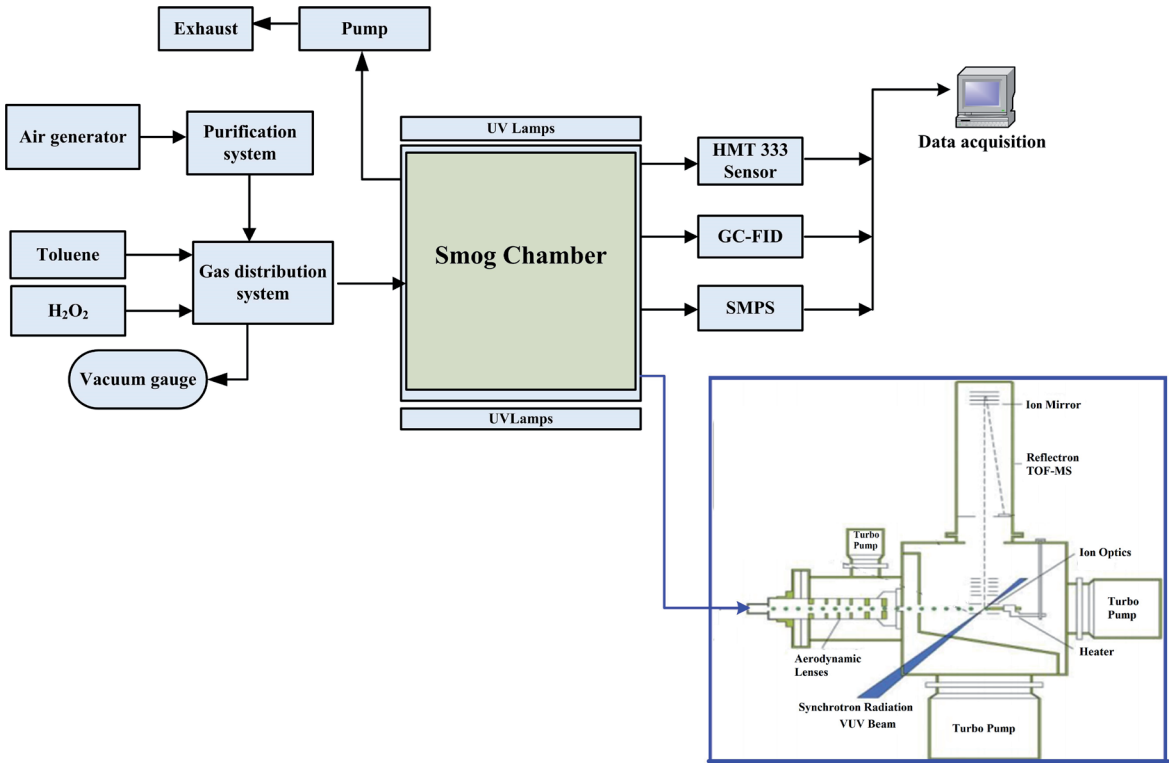

Fig. 1. Schematic diagram of a smog chamber coupled with a vacuum ultraviolet photoionization aerosol mass spectrometer.

third of the volume was filled with clean air. Then, 1 μL of toluene and 10 μL of hydrogen peroxide solution were successively added to the liquid vaporization bottle in the gas distribution platform. After vaporization, the gaseous toluene and hydrogen peroxide mixture was filled into the chamber, followed by further filling to full volume with clean air. Subsequently, UV lights were switched on to illuminate hydrogen peroxide, generating OH radicals that initiated the photooxidation reaction of toluene. Concentrations of toluene and SOA particles were measured using GC-FID and SMPS. After the illumination ended, the chemical composition of SOA was detected online by VUV-PIAMS, just like the detection of toluene fine particles as mentioned above.

Offline Detection of Toluene SOA

After the illumination was completed, toluene SOA particles were also collected onto a polytetrafluoroethylene filter membrane (47mm, 0.2 μm pore size, Sigma-Aldrich Corporation, USA). After 30 min of ultrasonic treatment, the organic components were extracted into 2% methanol water solution to obtain the SOA extraction solution. The absorption spectra of the SOA extraction solution in the 200-600 nm range were measured using an ultraviolet-visible (UV-Vis) spectrometer (UV-6100S, Mapada Instruments, China). The SNR of full-spectrum scanning signals ranged from 200 to 1000 under standard test conditions. Also, the negative ion mass spectra of the SOA extraction solution were detected by high-performance liquid chromatography-mass spectrometer (LC-MS, Agilent 1200 and 6320, Agilent Technologies, USA). Due to the limitation of experimental conditions, no suitable chromatographic column was found to separate the organic components of toluene SOA extraction, and MS/MS verification was not carried out. According to the experimental results of Carlton et al. [27] and our previous studies [16, 25, 28], the electrospray negative ionization mode of LC-MS caused the sample molecule to lose a hydrogen ion and generate a deprotonated molecular ion peak ($[M\text{-}H]^-$), thereby offering molecular weight information for the sample component. This could be used for qualitative analysis of the organic components of the toluene SOA extraction solution. Thus, the SOA extraction solution was measured with no chromatography column attached, and was electrospray ionized and detected directly. The mobile phase was a mixture of methanol and ultra-pure water (volume ratio of 1:1) with a flow rate of 0.20 mL/min. The LC-MS employed electrospray ionization to measure the mass spectra of the SOA extraction solution, with the scanning range of 5~1700 amu and SNR maintained at 50-500 [16, 25, 28].

Results and Discussion

Mass Spectrographic Analysis of Toluene Fine Particles

Most chemical constituents of SOA have ionization energies ranging from 8.0 eV to 10.2 eV [23, 29]. The synchrotron radiation photon energy of 10.5 eV is slightly above this range, which enables efficient single-photon ionization for the majority of SOA species with high ionization efficiency (⩾80%). For organic compounds with ionization energies between 10.2 and 10.5 eV (trace organic components of SOA), a moderate ionization efficiency (40-60%) is obtained. However, organic compounds with ionization energies greater than 10.5 eV (non-SOA components) cannot be ionized. Also, photon energy of 10.5 eV is a typical soft ionization condition. Photon energy higher than 11 eV will cause severe molecular fragmentation and generate numerous fragment ions, complicating component identification and quantification. In contrast, energy below 10.0 eV fails to ionize some SOA components with relatively high ionization energy, leading to signal loss [22, 24, 25, 29]. Thus, 10.5 eV was specifically selected for SOA measurements.

The VUV beamlines at Hefei National Synchrotron Radiation Laboratory were optimized for the 10-11 eV range, with high flux and minimal higher-order harmonic contamination. In our previous experiments, by adjusting the energy of synchrotron radiation photons, it was also found that 10.5 eV synchrotron radiation photons could ionize the organic components of SOA with minimal fragment generation [22, 24, 25]. To further confirm this and conduct a comparative analysis of chemical components of toluene SOA, toluene fine particles were first measured using VUV-PIAMS in real-time. As displayed in Fig. 1, particles passed through the aerodynamic lens, collided with the heated metal plate to volatilize into gas, and entered the ionization chamber. Subsequently, photoionization was carried out using synchrotron radiation photons with energies of 10.5, 13.0, and 15.5 eV, respectively, and the obtained mass spectra are shown in Fig. 2. When the photon energy was 10.5 eV, the molecular ion peak ($C_7H_8^+$, m/z = 92) and the protonated molecular ion peak ($C_7H_9^+$, m/z = 93) of toluene were measured. As photon energy continued to rise, toluene molecular ions underwent photodissociation, producing fragment ion peaks. Fragment peaks at m/z = 91 and 77 were detected under the photon energy of 13.0 eV. When the photon energy reached 15.5 eV, the intensities of the m/z = 91 and 77 fragment peaks observably increased. On the basis of the structure of the toluene molecule, mass peaks with m/z = 91 and 77 might be fragment peaks ($C_7H_7^+$ and $C_6H_5^+$) produced by the photodissociation of the toluene molecular ion peak, losing a hydrogen atom and a methyl group, respectively.

Fig. 3 shows the PIE curve of the toluene molecule ion ($C_7H_8^+$). The PIE curve of the ion peak typically

starts to rise from the baseline close to zero. Referring to our previous experimental studies [22, 24, 25], the "linear extrapolation method" was utilized to ascertain the sample's ionization potential (IP). The curve was divided into a low-efficiency zone (where the ionization efficiency approached zero) and a high-efficiency zone (where the ionization efficiency significantly increased). Linear fitting was performed on the high-efficiency region, the fitted line was extended, and the intersection point with the zero efficiency line was determined.

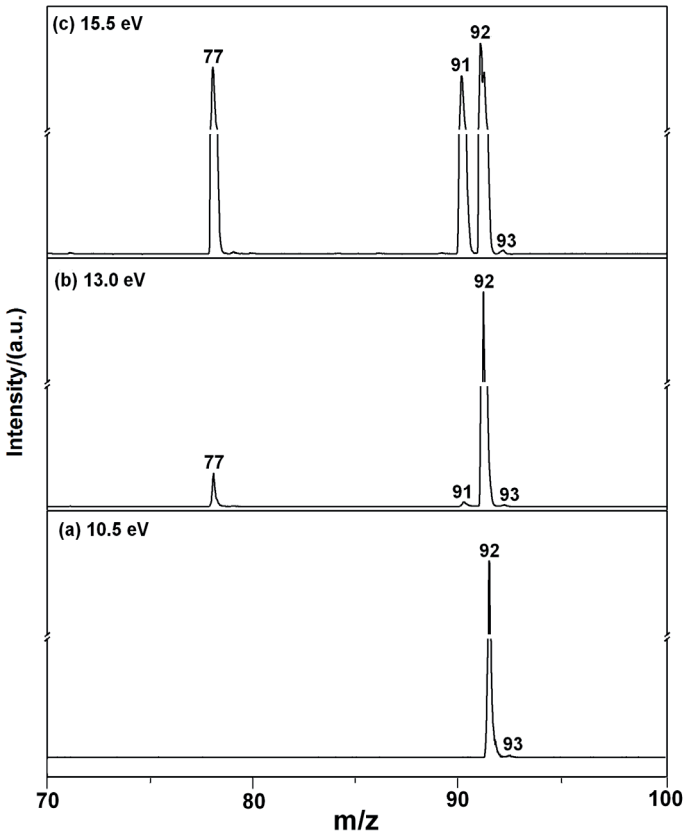

Fig. 2. Mass spectra of toluene fine particles at an energy of a) 10.5 eV, b) 13.0 eV, and c) 15.5 eV.

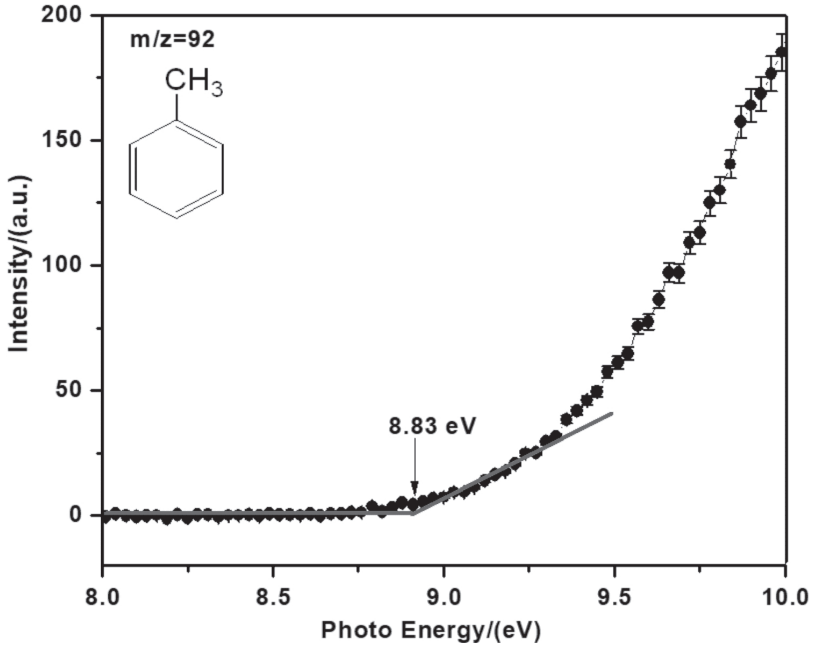

Fig. 3. Photoionization efficiency curve of toluene molecule ion ($C_7H_8^+$).

The photon energy corresponding to this intersection point was the sample's ionization potential. As shown in Fig. 3, the ionization efficiency significantly increased when the synchrotron radiation photon energy exceeded 9.0 eV. The linear fit was performed on the high-efficiency region, and the extended fitting line intersected the zero efficiency line at the point of 8.83 eV. Therefore, the ionization potential of the toluene molecule was determined to be IP($C_7H_8^+$)=(8.83±0.03) eV. This value was relatively close to the IP obtained by Lu et al. [30] using photoionization technology (PI) (8.83 eV), by Klasinc et al. [31] with photoelectron spectroscopy (PE) (8.79 eV), by Selim and Helal [32] utilizing electron impact ionization (EI) (8.80±0.07 eV), and by Kobayashi et al. [33] based on charge transfer spectroscopy (CTS) (8.91 eV). Based on the above analysis, it could be concluded that when the photon energy of the synchrotron radiation was 10.5 eV, toluene and other organic compounds were ionized, and the possibility of dissociation of the parent molecules was minimized.

It is worth noting that the heated plate could induce thermal decomposition, and some observed fragments may originate from thermal desorption products. Most SOA components (aromatics, carboxylic acids, aldehydes, ketones, esters, and common oligomers) have thermal decomposition thresholds (⩾180ºC) under vacuum and short residence times (<1 s) [34]. According to the experimental results of Gloaguen et al. [35], Zhang et al. [36], and our previous studies [22, 24, 25, 37], the 180ºC heated plate does not induce significant thermal decomposition of SOA components, and the observed fragment ions exhibit identical ionization thresholds to their parent molecules, demonstrating that fragments were predominantly from soft VUV photoionization rather than thermal desorption artifacts. To further confirm this, the temperature of the heated plate was set to 150, 180, and 210ºC in sequence. The mass spectra of toluene particles measured at a photon energy of 10.5 eV, shown in Fig. S1 in the Supplementary Information, were basically similar to those in Fig. 2a), both showing only the main molecular ion peak of toluene and no other fragment peaks. This confirmed that under the condition of a heated plate at 180ºC, thermal decomposition was essentially not induced, and the fragment ions detected in the experiment were mainly generated by photoionization. Therefore, the temperature of the heated plate was set to 180ºC for measuring the chemical components of toluene SOA in this study.

Mass Spectrographic Analysis of Toluene SOA Particles

Wall-loss correction is the prerequisite for measuring the concentration of SOA. Based on our previous experiments [16, 25, 26], the detailed explanation of how wall-loss correction was offered in the Supplementary Information. Particle wall loss was dependent on loss coefficient $k_{dep}(d_p)$, which was related to particle diameter (d_p) as follows [38]:

$$k_{dep}(d_p) = ad_p^b + c/d_p^d$$

The parameters a, b, c, and d were obtained from Fig. S2 shown in Supplementary Information as 4.17×10^{-13}, 4.66, 10.18, and 0.75, respectively. The concentration of SOA in the chamber was measured using SMPS, and the wall effect was corrected according to the above parameters. The variation of SOA mass concentration with photooxidation time is shown in Fig. 4. The reaction between toluene and OH radicals produced semi- and non-volatile products, which formed SOA after reaching their saturated vapor pressure. Some toluene needed to be consumed within 15 minutes to reach the saturation vapor pressure of the product; therefore, the SOA concentration was only 7 μg/m^3. Then, the amount of gaseous products continued to increase, and the SOA concentration swiftly rose from 28 μg/m^3 to 197 μg/m^3 during the 30-150 minute period. Although no toluene was measured by GC-FID after 180 minutes, the SOA concentration detected by SMPS reached 228 μg/m^3. Subsequently, as the toluene reaction was complete, the SOA concentration corrected for the wall effect tended to stabilize [16, 25, 26]. Aerosol yield is an important parameter in a chamber experiment. The aerosol yield (Y) was defined as $Y = \Delta M_o/\Delta ROG$, where ΔM_o (μg/m^3) was the mass concentration of organic aerosol produced by the reaction, and ΔROG (μg/m^3) represented the gas concentration consumed by the reaction [8, 9]. The yields of toluene SOA measured in three experiments were 8.66%, 8.72%, and 8.69%, respectively, with a standard deviation of 0.03%. At the confidence level of 95%, the obtained yield of toluene SOA was (8.69±0.07)%, which was comparable to the yield of toluene SOA (8.5-11.4%) reported by Srivastava et al. [8].

After 4 hours of photooxidation, chemical components of toluene SOA were detected online utilizing VUV-PIAMS. Fig. 5 illustrates the mass spectra for toluene SOA obtained at a synchrotron radiation photon energy of 10.5 eV. The ion peaks generated by ionization of SOA constituents were more abundant, and compared to Fig. 2, mass peaks such as m/z = 58, 64, 72, 74, 88, 94, 106, 108, 122, and 138 were newly added. This indicated that new photooxidation products had formed. Because of the relatively weak intensity of some peaks (m/z = 58, 74, 88, and 138), PIE curves for these peaks could not be acquired. The PIE curves for m/z = 64, 72, 94, 106, 108 and 122 obtained in the 7.5-11.5 eV range were displayed in Fig. 6. Based on our previous experiments [22, 24, 25], the following steps were adopted to qualitatively analyze the chemical components of toluene SOA: (1) By combining the m/z value of each peak and molecular weight (Mw) of the possible product generated by the reaction of toluene with OH radicals, the possible organic products corresponding to each mass peak were qualitatively

inferred. (2) For the PIE curve, the "linear extrapolation method" was utilized to ascertain the sample's IP, and it was compared with the IP of the speculated component provided by previous literature studies to determine the product information. Different organic compounds have different IP values. The obtained IP could be used to qualitatively determine the organic product and infer its structure [20, 21]. (3) The IP of the speculated component was achieved through quantum chemical calculations, and then compared with the experimentally measured and previously reported values to further confirm the product information.

The mass peaks at m/z = 64, 72, 94, 106, 108, and 122 shown in Fig. 5 had m/z values equal to the molecular weights of furan, methylglyoxal, phenol, benzaldehyde, methylphenol, and benzoic acid produced by the reaction of toluene with OH radicals. These were speculated to be molecular ion peaks for these products. The IPs of components corresponding to m/z = 64, 72, 94, 106 and 122 were measured to be (8.92±0.03) eV, (9.63±0.03) eV, (8.53±0.03) eV, (9.45±0.03) eV, and (9.26±0.03) eV, respectively (see Fig. 6(a-d) and f)), which were consistent with the IPs for furan, methylglyoxal, phenol, benzaldehyde, and benzoic acid reported by Klapstein

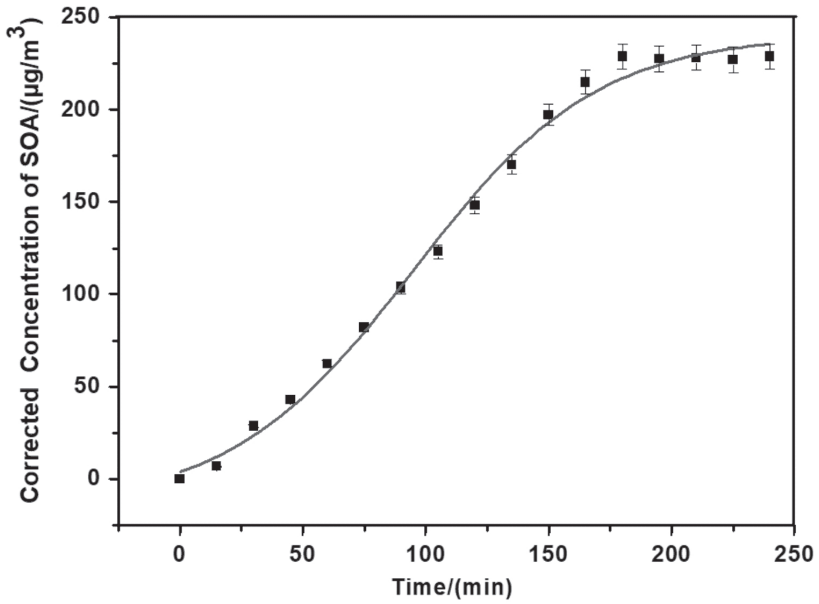

Fig. 4. Corrected concentration of toluene SOA versus photooxidation time.

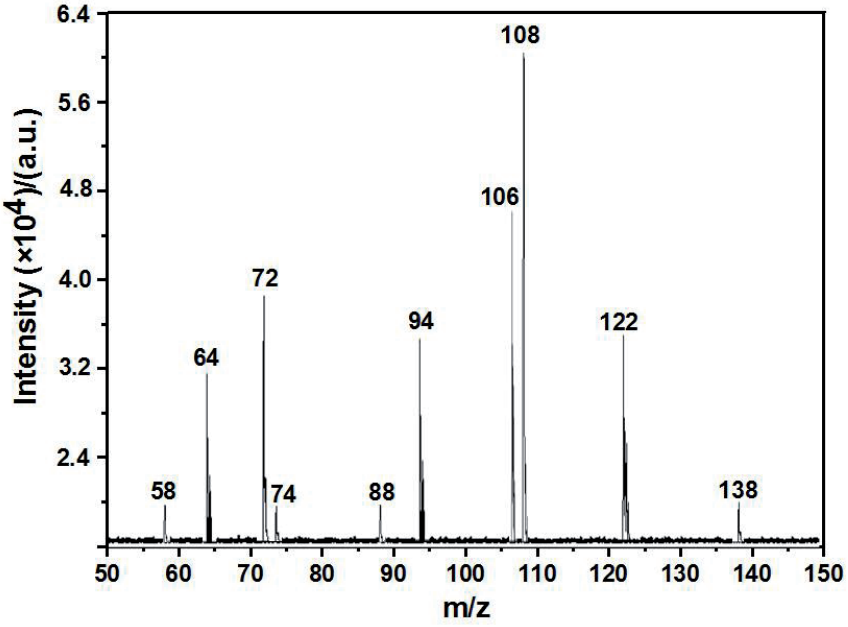

Fig. 5. Mass spectra of toluene SOA particles at an energy of 10.5 eV.

[39], Reed and Brand [40], Watanabe [41], Behan et al. [42], and Klasic et al. [31] (see Table 1). Thus, mass peaks with m/z = 64, 72, 94, 106, and 122 were identified as furan, methylglyoxal, phenol, benzaldehyde, and benzoic acid molecular ion peaks. It is worth noting that the PIE curve of the m/z = 108 ion peak presented a stepped pattern. The high-efficiency regions for each step were fitted linearly, and the intersection point of the extended fitting line with the zero efficiency line (or the parallel line of the zero efficiency line) was obtained, resulting in two IPs of (8.28±0.03) eV and (8.93±0.03) eV (see Fig. 6e)). The IP of 2-methylphenol was measured to be (8.24±0.02) eV by Maier and Turner [43], while the IP of 4-methylphenol was determined to be 8.97 eV by Crable and Kearns [44]. It could be inferred that the m/z = 108 ion peak corresponded to the two isomers of 2-methylphenol and 4-methylphenol. It should be noted that other mass peaks might also contain isomeric components. However, for the PIE curves of the other peaks shown in Fig. 6, only one IP was measured, which might be because the concentration of the corresponding isomeric component was too low and its IP could not be measured.

To further confirm the composition information of toluene SOA, theoretical calculations on the IPs of components were conducted. According to the theory of quantum chemistry, the IP of an organic compound (R) can be calculated using the following formula [20-22]:

$$R \rightarrow R^+ + e$$
$$IP(R) = E_0(R^+) - E_0(R)$$

where $E_0(R)$ and $E_0(R^+)$ represent the energies of the organic compound (R) and its molecular ion (R^+), respectively. Based on the computational methods developed in our previous studies [22, 24, 25], systematic conformational searches were first performed for the neutral organic compound (R) and its molecular ion (R^+) using the MMFF94 molecular mechanics force field [45]. All low-energy conformers within 10 kJ/mol relative to the global minimum were screened out for subsequent quantum chemical calculations. The geometries of all qualified conformers were fully optimized at ωB97X/6-31+G(d,p) with Gaussian 09 [46]. Vibrational frequency analysis was carried out at the same theoretical level to verify that all optimized structures correspond to true energy minima (no imaginary frequencies), and harmonic vibrational frequencies as well as unscaled zero-point vibrational energies (ZPE) (E_{ZPE}) were simultaneously obtained. Subsequently, high-precision single-point energy ($E_{CCSD(T)}$) calculations were conducted at the CCSD(T)/cc-pVTZ level on the most stable conformers from geometry optimization. A standard scaling factor of 0.9806 was used to account for anharmonicity and systematic errors in the harmonic approximation. The accurate energy values of $E_0(R)$ and $E_0(R^+)$ were computed as: $E_0 = E_{CCSD(T)} + E_{ZPE} * 0.9806$. Then, the ionization potential of the organic compound (IP(R)) was determined by calculating the difference between the two ($E_0(R^+)$-$E_0(R)$) [24, 25].

The ωB97X/6-31+G(d,p) method yielded relative energies with an uncertainty of ±(0.5-1.0) kJ/mol [47], while the CCSD(T)/cc-pVTZ method presented a typical uncertainty of ±(1-2) kJ/mol for small-to-medium organic molecules [48]. The uncertainty introduced by ZPE scaling and correction was less than ±0.5 kJ/mol [49]. Thus, the overall combined uncertainty of the present computational scheme was estimated to be ±(1.7-3.5) kJ/mol. Such calculation errors were acceptable and did not affect the reliability of the ionization potential results in this study. As shown in Table 1, the calculated IPs of furan, methylglyoxal, phenol, benzaldehyde, 2-methylphenol, 4-methylphenol, and benzoic acid were in good agreement with the values from previous literature [31, 39-44] and the IPs measured in this study. This further confirmed that peaks at m/z = 64, 72, 94, 106, 108, and 122 refer to molecular ion peaks of these reaction products.

Offline Verification of Toluene SOA Particle Components

According to the theoretical calculations by Suh et al. [50] and the experimental results of Li et al. [7], Srivastavad et al. [8], Lin et al. [51], and Jang et al. [52], the OH radicals initiate the photooxidation of toluene via methyl hydrogen abstraction and addition reactions

Table 1. Ionization potential of m/z = 64, 72, 94, 106, 108 and 122 obtained by experiment (Exp.), theoretical calculation (Cal.), and the possible formulas and species information for these ion peaks.

M/z	Formula	Species	Exp. (eV)	Cal. (eV)	Reference (eV)
64	C_4H_4O	Furan	8.92±0.03	8.91	8.90 [39]
72	$C_3H_4O_2$	Methylglyoxal	9.63±0.03	9.65	9.60±0.06 [40]
94	C_6H_6O	Phenol	8.53±0.03	8.52	8.50±0.01 [41]
106	C_7H_6O	Benzaldehyde	9.45±0.03	9.48	9.49 [42]
108	C_7H_8O	2-Methylphenol 4-Methylphenol	8.28±0.03 8.93±0.03	8.27 8.92	8.24±0.02 [43] 8.97 [44]
122	$C_7H_6O_2$	Benzoic acid	9.26±0.03	9.32	9.3 [31]

to the benzene ring. As shown in Fig. 7, after the OH radicals extracted a methyl hydrogen atom, the oxygen molecule promptly added to the carbon atom to form the peroxy radical. This peroxy radical then reacted with NO and the oxygen molecule to produce benzaldehyde. Under the initiation of the OH radicals, benzaldehyde could further react with the oxygen molecule to generate benzoic acid [7, 8, 52]. OH radicals were mainly added to the ipso, ortho, and para carbon atoms of the methyl group, forming ipso-OH-toluene, ortho-OH-toluene, and para-OH-toluene adducts. The ipso-OH-toluene adduct could dealkylate and lose a methyl substituent on the benzene ring to generate phenol. Meanwhile, oxygen molecules extracted the hydrogen from the carbon atom associated with the OH group in ortho-OH-toluene and para-OH-toluene adducts to yield 2-methylphenol and 4-methylphenol [7, 8, 51, 52].

In addition, an oxygen molecule could be added to the ipso carbon atom of the methyl group in the ortho-OH-toluene adduct to form ortho-OH toluene peroxy radical (RO_2), whose oxygen atom was extracted by NO to produce ortho-OH-toluene alkoxy radical (RO)

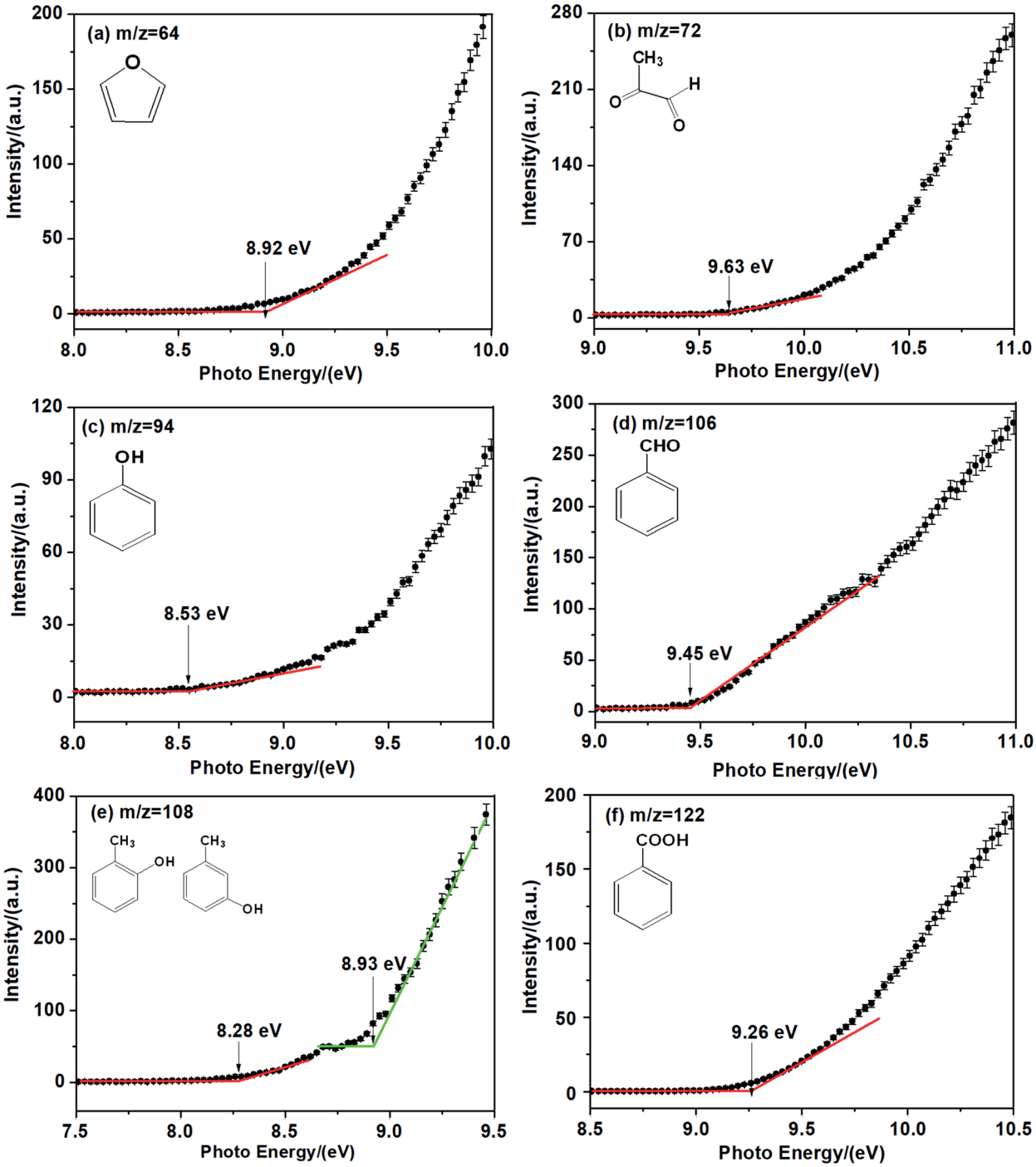

Fig. 6. Photoionization efficiency curves of a) m/z = 64, b) m/z = 72, c) m/z = 94, d) m/z = 106, e) m/z = 108, and f) m/z = 122.

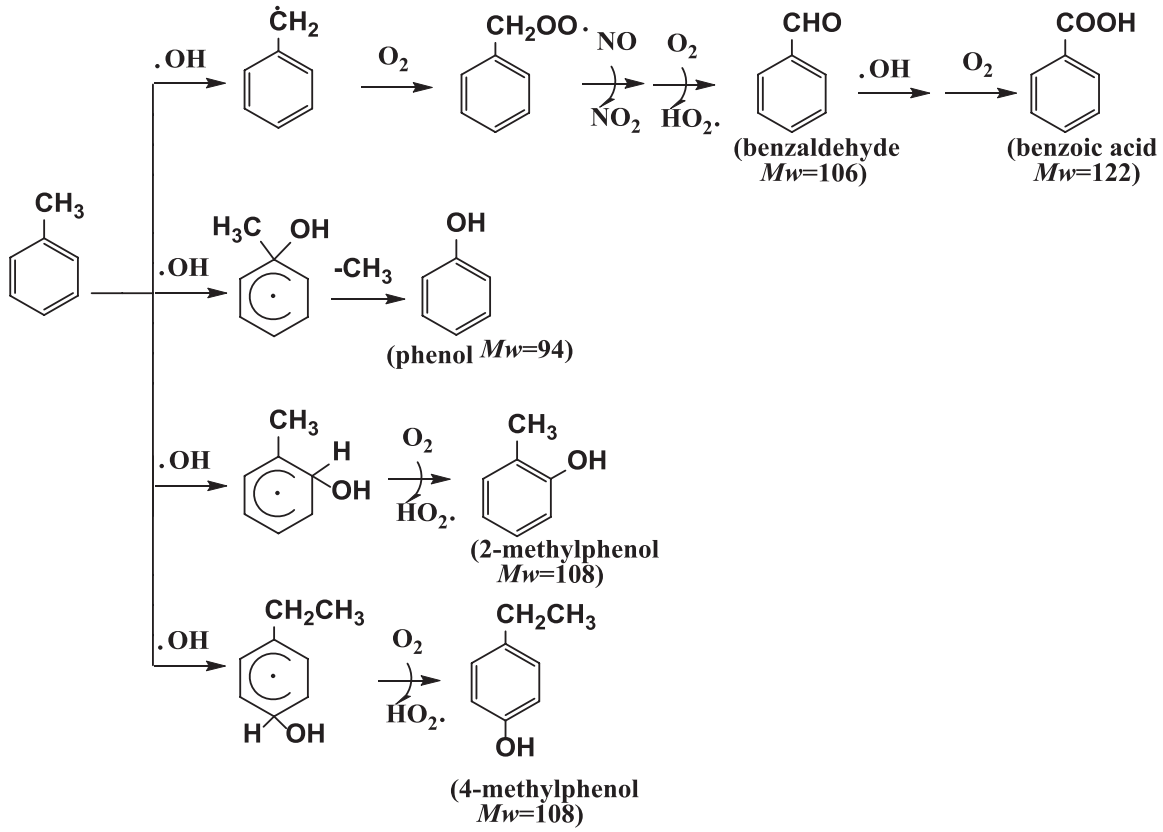

Fig. 7. Suggested mechanism of the reaction of OH radicals with toluene to form phenol, benzaldehyde, methylphenol, and benzoic acid.

(see Fig. 8a)). The oxygen atom of the alkoxy radical could attack the carbon on the benzene ring, forming a wheelchair-shaped intermediate that underwent a series of reactions to generate furan and methylglyoxal. Also, the ortho-OH toluene peroxy radical could involve the formation of a bicyclic radical with an O-O bridge across the benzene ring, to which an oxygen molecule was added to generate a bicyclic peroxy radical subsequently. The formed bicyclic peroxy radical reacted with NO to produce bicyclic alkoxy radical, which underwent cleavage of O-O bond and C-C bond of benzene ring to yield methylglyoxal and 2-butenedial [7, 8, 51, 52]. Therefore, furan, methylglyoxal, phenol, benzaldehyde, methylphenol, and benzoic acid were major photooxidation products of toluene. They were ionized to form mass peaks at m/z = 64, 72, 94, 106, 108, and 122 as illustrated in Fig. 5.

According to the research results of Molteni et al. [53] and Dong et al. [54], the H-transfer and cyclization reactions jointly promoted the autooxidation reaction of toluene. As illustrated in Fig. 8a), for the ortho-OH toluene peroxy radical formed by the reaction of toluene with the OH radical and oxygen, the hydrogen on the carbon atom adjacent to the peroxy group was transferred to the terminal oxygen atom of the peroxy group, and the oxygen molecule immediately attached to the carbon atom, undergoing the cyclization reaction to form a bicyclic radical subsequently. This bicyclic radical continued to react with the oxygen molecule to produce a bicyclic peroxy radical, which further reacted with the HO_2 radical to generate low-volatility highly oxygenated organic molecule (HOM) products. It is worth noting that the generated methylglyoxal and other dialdehydes could undergo acid-catalyzed hydration and oligomerization reactions to form oligomer products. As shown in Fig. 8b), the acid-catalyzed hydration reaction of methylglyoxal generated diol products, which underwent self-reactions to yield a cyclic dimer. This cyclic dimer could further lead to oligomerization reactions to produce cyclic trimers, tetramers, and other oligomer products [7, 55]. Owing to HOMs and cyclic oligomer products having lower volatility and higher ionization energy [20], the molecular ion peaks of these lower volatility products could not be detected using VUV-PIAMS in this study. Future experiments can increase the temperature of the metal plate and the photon energy of the synchrotron radiation to measure these lower volatility products.

UV-Vis absorption spectra of the toluene SOA extraction solution are shown in Fig. 9. There were no absorption peaks in the visible light range of 400-600 nm, but there was a strong band at 210 nm. This band was a characteristic absorption produced by the n→π* transition of the carbonyl group [27]. In addition, there was a characteristic absorption peak of a phenolic compound near 277 nm [56]. These confirmed that phenolic and carbonyl products were major components

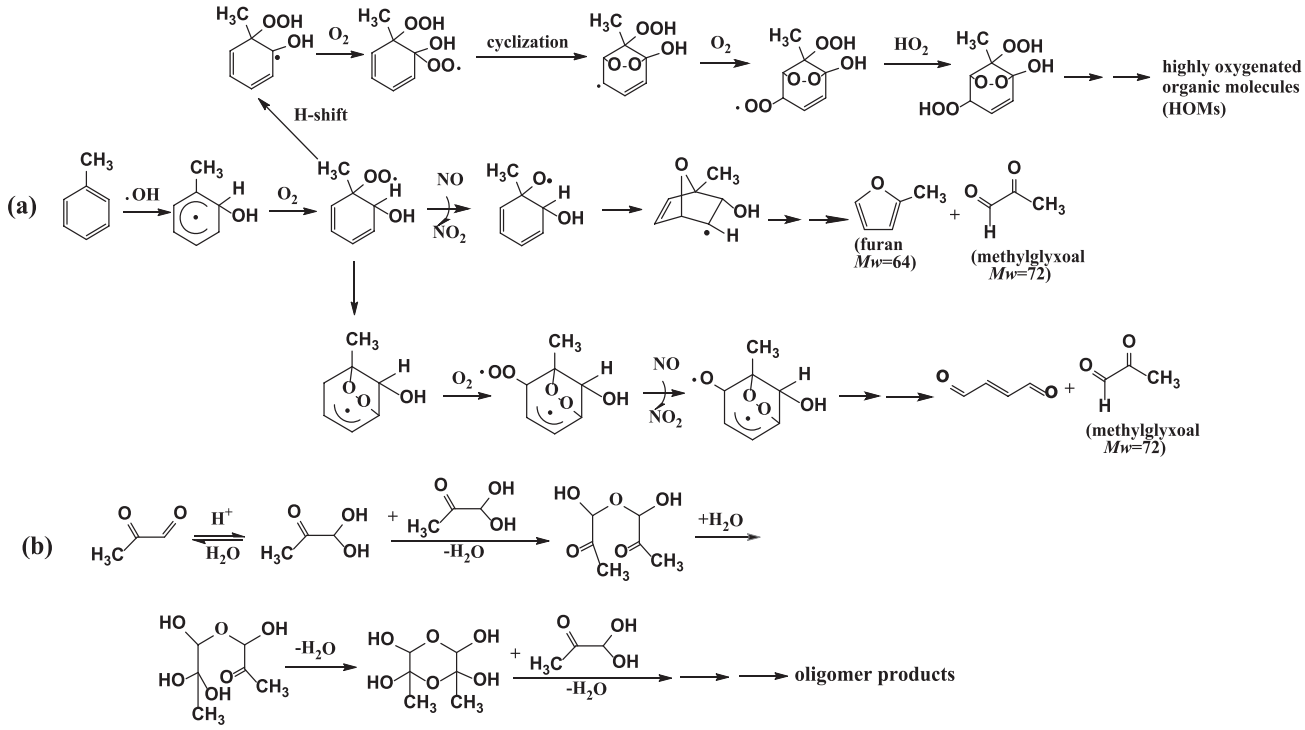

Fig. 8. Suggested mechanism of the reaction of OH radicals with toluene to form furan, methylglyoxal, highly oxygenated organic molecules, and oligomer products.

of toluene SOA. The negative ion mass spectra for the SOA extraction solution displayed in Fig. 10 contained strong ion peaks with m/z = 63, 71, 93, 105, 107, and 121. As suggested by Carlton et al. [27], electrospray negative ionization mode could offer molecular weight information about the sample components via the deprotonated molecular ion peak ($[M\text{-}H]^-$). Based on the suggested reaction mechanism and molecular weight (Mw) information of the products formed from the reactions of toluene with OH radicals shown in Fig. 7 and Fig. 8, these ion peaks corresponded to furan (Mw = 64, m/z = 63), methylglyoxal (Mw = 72, m/z = 71), phenol (Mw = 94, m/z = 93), benzaldehyde (Mw = 106, m/z = 105), methylphenol (Mw = 108, m/z = 107), and benzoic acid (Mw = 122, m/z = 121).

According to the online detection by VUV-PIAMS and offline verification using UV-Vis absorption spectroscopy and electrospray ionization

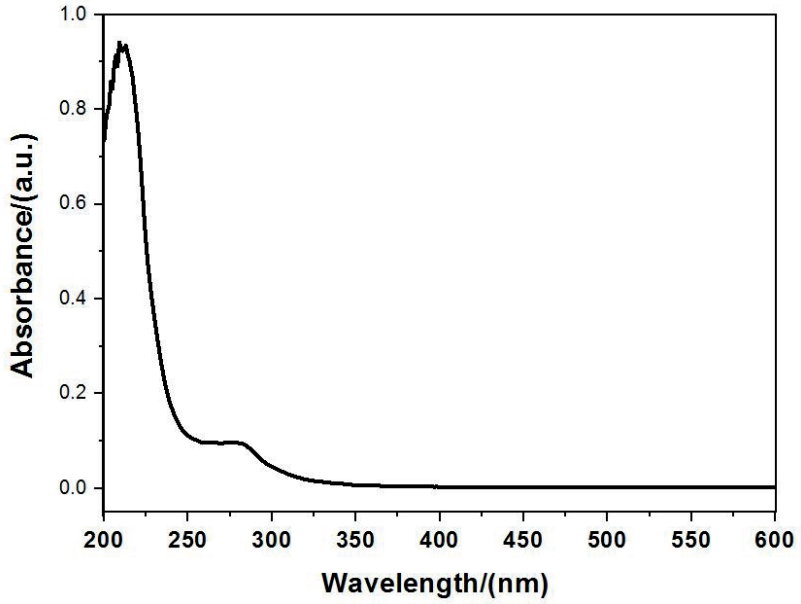

Fig. 9. UV-Vis absorption spectra of the toluene SOA extraction solution.

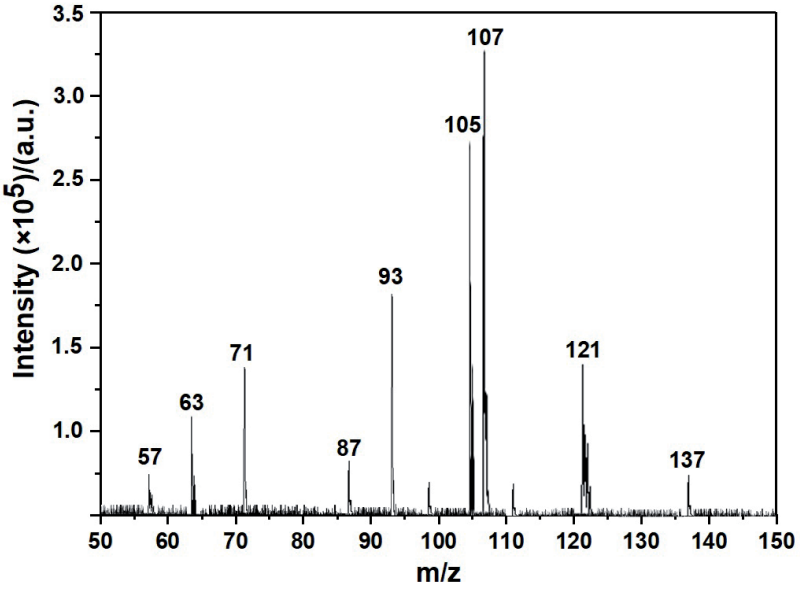

Fig. 10. Negative ion mass spectra of the toluene SOA extraction solution.

mass spectrometry, referring to the possible reaction mechanisms of toluene with OH radicals, it could be confirmed that furan, methylglyoxal, phenol, benzaldehyde, methylphenol, and benzoic acid were major components of toluene SOA. This was consistent with product information measured in photooxidation experiments of toluene performed by Li et al. [7], Srivastava et al. [8], Lin et al. [51], and Jang et al. [52]. It is worth noting that the area of each ion peak in the mass spectra of toluene SOA can roughly determine the relative abundances of the products and the generated quantity ratio of each product. The proportion of the product corresponding to a certain ion peak can be obtained by dividing the area of that ion peak by the total area of all ion peaks [20, 22, 25]. Based on the area of each ion peak in Fig. 5, it was found that methylphenol, benzaldehyde, benzoic acid, methylglyoxal, phenol, furan, and unidentified components accounted for 21.4%, 17.1%, 15.7%, 14.3%, 12.9%, 11.4%, and 7.2% of the measured components, respectively. The generated quantity ratio of methylphenol, benzaldehyde, benzoic acid, methylglyoxal, phenol, and furan was 15: 12: 11: 10: 9: 8.

Although no new products or mechanisms were identified, two isomers of 2-methylphenol and 4-methylphenol were first detected online in this study. It is worth mentioning that Sato et al. [57] have measured the mass spectra of toluene SOA using an Aerodyne aerosol mass spectrometer (AMS), which mainly contained fragment peaks such as m/z = 18, 29, and 44 (see Fig. S3 in Supplementary Information), generated from the dissociation of organic compounds like aldehydes, ketones, and carboxylic acids. In contrast, the mass spectra of toluene SOA measured by VUV-PIAMS, shown in Fig. 5, mainly contained molecular ion peaks of organic components. By combining the IP obtained from the PIE curve displayed in Fig. 6, furan, methylglyoxal, phenol, and other products were directly identified.

ESI-MS provided protonated ion peaks for the components of toluene SOA extraction (as shown in Fig. 10), but it was unable to distinguish the isomeric components corresponding to the mass peak. For instance, for the deprotonated ion peak of m/z = 107, only methylphenol could be identified. On the contrary, VUV-PIAMS detected a molecular ion peak of methylphenol at m/z = 108, measured its PIE curve, and obtained two IPs of (8.28±0.03) eV and (8.93±0.03) eV (see Fig. 6e)), corresponding to the IP of 2-methylphenol and 4-methylphenol, respectively. It could be inferred that the m/z = 108 ion peak corresponded to the two isomers of 2-methylphenol and 4-methylphenol. Compared to AMS and ESI-MS, VUV-PIAMS online detection, as a "soft ionization" technology, could minimize the possibility of dissociation for aerosol component molecules by controlling the photon flux and attaining molecular ion peaks of the components. By scanning the synchrotron wavelength, the PIE curve was obtained, and the structural information of the measured components was obtained based on the ionization potential. VUV-PIAMS can overcome cumbersome preparation procedures, time-consuming processes, potential secondary pollution, and other disadvantages of offline detection. It is a useful tool for measuring the chemical composition of SOA particles and revealing their formation processes.

It should be noted that the total carbon mass of initial toluene was partitioned into four components: residual gaseous toluene, gas-phase oxidation intermediates, particulate SOA mass, and chamber wall loss mass. VUV-PIAMS primarily detected molecular ions with minimal fragmentation, but it might miss highly

oxygenated species (low volatility but poor ionization efficiency at typical VUV energies) and gas-phase oxidation intermediates that did not partition to the aerosol phase. Furthermore, due to experimental limitations, it was currently impossible to measure the loss of toluene caused by the wall effect. Therefore, carbon mass balance analysis and concentration estimates were not conducted in this study. Subsequent experiments can delve into carbon mass balance analysis and product concentration measurements to further determine the atmospheric mechanism of toluene photooxidation.

Conclusions

VUV-PIAMS based on synchrotron radiation was combined with a smog chamber to conduct online measurement of SOA generated by the photooxidation of toluene. The obtained mass spectra of toluene SOA mainly presented ion peaks of m/z = 64, 72, 94, 106, 108, and 122. The PIE curve of each ion peak within the 7.5-11.5 eV synchrotron radiation photon range was measured, and thereby the ionization potential of each mass peak was acquired. Through the analysis of measured ionization potential, quantum chemical calculations, offline measurements using ultraviolet-visible absorption spectroscopy, and electrospray ionization mass spectrometry, furan, methylglyoxal, phenol, benzaldehyde, 2-methylphenol, 4-methylphenol, and benzoic acid were identified as the main components of toluene SOA. Based on the areas of the mass peaks, methylphenol, benzaldehyde, benzoic acid, methylglyoxal, phenol, furan, and unidentified components accounted for 21.4%, 17.1%, 15.7%, 14.3%, 12.9%, 11.4% and 7.2% of the measured components, respectively. The generated quantity ratio of methylphenol, benzaldehyde, benzoic acid, methylglyoxal, phenol, and furan was 15:12:11:10:9:8. VUV-PIAMS can minimize the formation of fragment ions to the greatest extent possible. The ionization potential of each mass peak is obtained through its PIE curve, and the component structural information can be analyzed; the isomeric components can also be distinguished. VUV-PIAMS can overcome the disadvantages of offline detection, which can be used for the online measurement of SOA.

Acknowledgments

Our work was supported by the Natural Science Foundation of Fujian Province of China (No. 2025J01972) and the National Natural Science Foundation of China (No. 42275136). The authors thank Michael Nusbaum from the Department of English, Xiamen University, Tan Kah Kee College for language edits. The authors also express their gratitude to the referees for their valuable comments.

Conflict of Interest

The authors declare no conflict of interest.

References

1. OLIVEIRA K., GUEVARA M., JORBA O., PETETIN H., BOWDALA D., TENA C., PINTO G.M., LÓPEZ F., GARCÍA-PANDO C.P. On the uncertainty of anthropogenic aromatic volatile organic compound emissions: Model evaluation and sensitivity analysis. Atmospheric Chemistry and Physics, **24** (12), 7137, **2024**.
2. ZHAO Y., WANG M.L., ZHU R.C., WEI Y.B., HE L.Q., HU J.N., LAI Y.T., SU S. Volatile organic compound emissions from light-duty vehicles: Effects of aromatic and olefin compositions in gasoline. Fuel, **407**, 137388, **2026**.
3. DANTAS G., GORNE I., DA SILVA C.M., ARBILLA G. Benzene, toluene, ethylbenzene, and xylene (BTEX) concentrations in urban areas impacted by chemical and petrochemical industrial emissions. Bulletin of Environmental Contamination and Toxicology, **108** (2), 204, **2022**.
4. JAYARAJ S., NAGENDRA S.M.S. An assessment of atmospheric concentrations and spatiotemporal variation of BTEX and associated pollutants in India. Journal of Environmental Sciences, **150**, 230, **2025**.
5. SAEED M., MALEKMOHAMMADI B., TAJALLI S. Interaction of benzene, toluene, ethylbenzene, and xylene with the human body: Insights into characteristics, sources, and health risks. Journal of Hazardous Materials Advances, **16**,100459, **2024**.
6. ZHANG D.H., TANG X.C., LIU X.B., HE Z.X., WANG S.H. Health hazards of occupational exposure to benzene, toluene, and xylene (BTX) and the role of Vanin-1: A populational-based study. International Archives of Occupational and Environmental Health, **99** (1), 4, **2026**.
7. LI Y.X., ZHAO J.Y., WANG Y., SEINFELD J.H., ZHANG R.Y. Multigeneration production of secondary organic aerosol from toluene photooxidation. Environmental Science & Technology, **55** (13), 8592, **2021**.
8. SRIVASTAVA D., LI W.R., TONG S.R., SHI Z.B., HARRISON R.M. Characterization of products formed from the oxidation of toluene and m-xylene with varying NO*x* and OH exposure. Chemosphere, **334**, 139002, **2023**.
9. URUCI P., FLOROUL K., PAGLIONE M., KALTSONOUDIS C., PICQUET-VARRAULT B., DOUSSIN J.F., CAZAUNAU M., LESKINEN A., HAO L.Q., VIRTANEN A., BELL D.M., MUTZEL A., MOTHES F., HERRMANN H., RODENAS M., MUÑOZ A., FUCHS H., BOHN B., NEHR S., ALFARRA M.R., VOLIQTIS A., MCFIGGANS G., PATROESCU-KLOTZ I.V., ILLMANN N., PANDIS S.N. Toluene photo-oxidation and secondary organic aerosol formation: EUROCHAMP-2020 multi-chamber experiments. Journal of Atmospheric Chemistry, **82** (2), 20, **2025**.
10. MOISE T., FLORES J.M., RUDICH Y. Optical properties of secondary organic aerosols and their changes by chemical processes. Chemical Reviews, **115** (10), 4400, **2015**.
11. PENG X., XIE T.T., TANG M.X., CHENG Y., PENG Y., WEI F.H., CAO L.M., YU K.Y., DU K., HE L.Y., HUANG X.F. Critical role of secondary organic aerosol in urban atmospheric visibility improvement identified by machine

learning. Environmental Science & Technology Letters, **10** (11), 976, **2023**.
12. LIU F.B., XU T.C., NG N.L., LU H. Linking cell health and reactive oxygen species from secondary organic aerosols exposure. Environmental Science & Technology, **57** (2), 1039, **2023**.
13. MANDAL D., CHAKRABORTY A., TRIPATHI S. Spatial heterogeneity of indoor carbonaceous aerosol levels and characteristics: Comparison with the outdoors and implications for secondary organic aerosol formation and health effects. Journal of Atmospheric Chemistry, **82** (2), 11, **2025**.
14. KIM H., KANG D., JUNG H.Y., JEON J., LEE J.Y. Review of smog chamber experiments for secondary organic aerosol formation. Atmosphere, **15** (1), 115, **2024**.
15. KUMAR V., SLOWIK J.G., BALTENSPERGER U., PREVOT A.S.H., BELL D.M. Time-resolved molecular characterization of secondary organic aerosol formed from OH and NO_3 radical initiated oxidation of a mixture of aromatic precursors. Environmental Science & Technology, **57** (31), 11572, **2023**.
16. WANG W.C., HUANG M.Q., HU H.M., ZHAO W.X., HU C.J., GU X.J., ZHANG W.J. Characterization of chemical components and optical properties of toluene secondary organic aerosol in presence of ferric chloride fine particles. Atmosphere, **14** (7), 1075, **2023**.
17. ZHU M.C., HUANG M.Q., ZHANG L.M., CAI S.Y., ZHAO W.X., HU C.J., GU X.J., ZHANG W.J. Experimental study on composition and optic of secondary organic aerosol generated by aqueous photoxidation of toluene in presence of copper ions. Polish Journal of Environmental Studies, **34** (1), 985, **2025**.
18. LASKIN J., LASKIN A., NIZKORODOV S.A. Mass spectrometry analysis in atmospheric chemistry. Analytical Chemistry, **90** (1), 166, **2018**.
19. CHEN J.D., JIANG S.P., YANG P.H., WANG L. Radiation source analysis of beamline stations at fourth-generation synchrotron light facility. Radiation Measurements, **189**, 107528, **2025**.
20. DANG M., LIU R.D., DONG F.S., LIU B., HOU K.Y. Vacuum ultraviolet photoionization on-line mass spectrometry: Instrumentation developments and applications. TrAC Trends in Analytical Chemistry, **149**, 116542, **2022**.
21. QIAN B., HU Y.H., XU M.G., YANG J.Z., LIU C.Y., PAN Y. Online exploring the gaseous oil fumes from oleic acid thermal oxidation by synchrotron radiation photoionization mass spectrometry. Journal of the American Society for Mass Spectrometry, **34** (12), 2680, **2023**.
22. FANG W.Z., GONG L., SHAN X.B., LIU F.Y., WANG Z.Y., SHENG L.S. Thermal desorption/tunable vacuum–ultraviolet time-of-flight photoionization aerosol mass spectrometry for investigating secondary organic aerosols in chamber experiments. Analytical Chemistry, **83** (23), 9024, **2011**.
23. CANAGARATNA M.R., MASSOLI P., BROWNE E.C., FRANKLIN J.P., WILSON K.R., ONASCH T.B., KIRCHSTRTTER T.W., FORTNER E.C., KOLB C.E., JAYNE J.T., KROLL J.H., WORSNOP D.R. Chemical compositions of black carbon particle cores and coatings via soot particle aerosol mass spectrometry with photoionization and electron ionization. The Journal of Physical Chemistry A, **119** (19), 4589, **2015**.
24. HU C.J., HUANG M.Q., LI B., WEI N.N., HU R.Z., MIKUŠKA P., VEČEŘA Z., GAI Y. B., LIN X.X., GU X.J., ZHAO W.X., ZHANG W.J., ZHANG H., CHEN J., LIU F.Y., SHAN X.B., SHENG L.S., LIU X.Y. On-line characterization of squalane aerosols using thermal desorption/tunable vacuum ultraviolet time-of-flight photoionization aerosol mass spectrometry. Talanta, **293**, 128044, **2025**.
25. HUANG M.Q., SHAN X.B., SHENG L.S., WANG Z.Y., HU C.J., GU X.J., ZHANG W.J. On-line measurement of styrene secondary organic aerosol using synchrotron radiation vacuum ultraviolet photoionization aerosol mass spectrometer. Chinese Journal of Analytical Chemistry, **52** (8), 1200, **2024**.
26. HUANG M.Q., XU J., CAI S.Y., LIU X.Q., HU C.J., GU X,J., FANG L., ZHANG W.J. Mass spectral analysis of the aged 1,3,5-trimethylbenzene secondary organic aerosol in the presence of ammonium sulfate seeds. Polish Journal of Environmental Studies, **26** (4), 1531, **2017**.
27. CARLTON A.G., TURPIN B.J., ALTIERI K.E., SEITZINGER S., REFF A., LIM H.J., ERVENS B. Atmospheric oxalic acid and SOA production from glyoxal: Results of aqueous photooxidation experiments. Atmospheric Environment, **41** (35), 7588, **2007**.
28. ZHANG W., HUANG M.Q., LU T.T., CAI S.Y., ZHAO W.X., HU C.J., GU X.J., ZHANG W.J. Characterization of nitro-aromatic compounds of ethylbenzene secondary organic aerosol with acidic sodium nitrate fine particles. Polish Journal of Environmental Studies, **31** (1), 451, **2022**.
29. ZANG X.Y., ZHANG Z.Y., WANG C., WANG T.T., ZHENG H.J., XIE H., YANG J.Y., DAI D.X., WU G.R., ZHANG W.Q., LI G., YANG X.M., JIANG L. Vacuum ultraviolet free-electron laser photoionization mass spectrometry of alpha-pinene ozonolysis. Chinese Journal of Chemical Physics, **35** (2), 281, **2022**.
30. LU K.T., EIDEN G.C., WEISSHAAR J.C. Toluene cation: Nearly free rotation of the methyl group. The Journal of Physical Chemistry, **96** (24), 9742, **1992**.
31. KLASINC L., KOVAC B. GUSTEN H. Photoelectron spectra of acenes. Electronic structure and substituent effects. Pure and Applied Chemistry, **55** (2), 289, **1983**.
32. SELIM E.T.M., HELAL A.I. The study of C_1-C_3 monosubstituted alkyl benzenes by the inverse convolution of first differential ionization efficiency curves. Organic Mass Spectrometry, **17** (11), 539, **1982**.
33. KOBAYASHI H., KOBAYASHI M., KAIZU Y. Molecular complexes of arenetri carbonylchromium. Bulletin of the Chemical Society of Japan, **46** (10), 3109, **1973**.
34. WEST C.P., HSU Y.J., MACFEELY K.T., HUSTON S.M., ARIDJIS-OLIVOS B.P., MORALES A.C., LASKIN A. Volatility measurements of individual components in organic aerosol mixtures using temperature-programmed desorption-direct analysis in real time-high resolution mass spectrometry. Analytical Chemistry, **95** (19), 7403, **2023**.
35. GLOAGUEN E., MYSAK E.R., LEONE S.R., AHMED M., WILSON K.R. Investigating the chemical composition of mixed organic-inorganic particles by "soft" vacuum ultraviolet photoionization: The reaction of ozone with anthracene on sodium chloride particles. International Journal of Mass Spectrometry, **258** (1-3), 74, **2006**.
36. ZHANG P., MA P.K., ZHANG H.X., SHU J.N., YANG B., LI Z. Application of VUV-PIMS coupled with GC-MS in chemical characterization, identification and comparative analysis of organic components in both vehicular-derived SOA and haze particles. Atmospheric Environment, **164**, 250, **2017**.
37. FANG W.Z., GONG L., ZHANG Q., CAO M.Q., LI Y.Q., SHENG L.S. Measurements of secondary organic aerosol

formed from OH-initiated photo-oxidation of isoprene using online photoionization aerosol mass spectrometry. Environmental Science & Technology, **46** (7), 3898, **2012**.
38. TAKEKAWA H., MINOURA H., YAMAZAK S. Temperature dependence of secondary organic aerosol formation by photo-oxidation of hydrocarbons. Atmospheric Environment, **37** (24), 3413, **2003**.
39. KLAPSTEIN D., MACPHERSON C.D., O'BRIEN R.T. The photoelectron spectra and electronic structure of 2-carbonyl furans. Canadian Journal of Chemistry, **68** (5), 747, **1990**.
40. REED R.I., BRAND J.C.D. Electron impact studies. Part 4. Glyoxal, methylglyoxal and diacetyl. Transactions of the Faraday Society, **54**, 478, **1958**.
41. WATANABE K. Ionization potentials of some molecules. The Journal of Chemical Physics, **26** (3), 542, **1957**.
42. BEHAN J.M., JOHNSTONE R.A.W., BENTLEY T.W. An evaluation of empirical methods for calculating the ionization potentials of substituted benzenes. Journal of Mass Spectrometry, **11** (2), 207, **1976**.
43. MAIER J.P., TURNER D.W. Steric inhibition of resonance studied by molecular photoelectron spectroscopy. Part 2. Phenylethylenes, Journal of the Chemical Society, Faraday Transactions 2: Molecular and Chemical Physics, **69**, 196, **1973**.
44. CRABLE G.F., KEARNS G.L. Effect of substituent groups on the ionization potentials of benzenes. The Journal of Physical Chemistry, **66** (3), 436, **1962**.
45. HALGREN T.A. Merck molecular force field. I. Basis, form, scope, parameterization, and performance of MMFF94. Journal of Computational Chemistry, **17** (5-6), 490, **1996**.
46. FRISCH M.J., TRUCKS G.W., SCHLEGEL H.B., SCUSERIA G.E., ROBB M.A., CHEESEMAN J.R., SCALMANI G., BARONE V., MENNUCCI B., PETERSSON G.A., NAKATSUJI H., CARICATO M., LI X., HRATCHIAN H.P., IZMAYLOV A.F., BLOINO J., ZHEN G., SONNENBERG J.L., HADA M., EHARA M., TOYOTA K., FUKUDA R., HASEGAWA J., ISHIDA M., NAKAJIMA T., HONDA Y., KITAO O., NAKAI H., VREVEN T., MONTGOMERY J.A.JR., PERALTA J.E., OGLIARO F., BEARPARK M., HEYD J.J., BROTHERS E., KUDIN K.N., STARVEROV V.N., KOBAYASHI R., NORMAND J., RAGHAVACHARI K., RENDELL A., BURANT J.C., IYENGAR S.S., TOMASI J., COSSI M., REGA N., MILLAM J.M., KLENE M., KNOX J.E., CROSS J.B., BAKKEN V., ADAMO C., JARAMILLO J., GOMPERTS R., STRATMANN R.E., YAZYEV O., AUSTIN A.J., CAMMI R., POMELLI C., OCHTERSKI J.W., MARTIN R.L., MOROKUMA K., ZAKRZEWSKI V.G., VOTH G.A., SALVADOR P., DANNENBERG J.J., DAPPRICH S., DANIELS A.D., FARKAS O., FORESMAN J.B., ORITIZ J.V., CIOSLOWSKI J., FOX D.J. Gaussian 09, Revision A.01, Gaussian Inc., Wallingford CT, **2009**.
47. CHAI J.D., HEAD-GORDON M. Long-range corrected hybrid density functionals with damped atom–atom dispersion corrections. Physical Chemistry Chemical Physics, **10** (44), 6615, **2008**.
48. SPIEKERMANN K., PATTANAIK L., GREEN W.H. High accuracy barrier heights, enthalpies, and rate coefficients for chemical reactions. Scientific Data, **9**, 417, **2022**.
49. IRIKURA K.K., JOHNSON III R.D., KACKER R.N., KESSEL R. Uncertainties in scaling factors for ab initio vibrational zero-point energies. The Journal of Chemical Physics, **130** (11), 114102, **2009**.
50. SUH I., ZHANG R.Y., MOLINA L.T., MOLINA M.J. Oxidation mechanism of aromatic peroxy and bicyclic radicals from OH-toluene reactions. Journal of the American Chemical Society, **125** (41), 12655, **2003**.
51. LIN P., LIU J.M, SHILLING J.E., KATHMANN S.M., LASKIN J., LASKIN A. Molecular characterization of brown carbon (BrC) chromophores in secondary organic aerosol generated from photo-oxidation of toluene. Physical Chemistry Chemical Physics, **17** (36), 23312, **2015**.
52. ANG M., KAMENS R.M. Characterization of secondary aerosol from the photo- oxidation of toluene in the presence of NO*x* and 1-propene. Environmental Science & Technology, **35** (18), 3626, **2001**.
53. MOLTENI U., BIANCHI F., KLEIN F., EL HADDAD I., FREGE C., ROSSI M.J., DOMMEN J., BALTENSPERGER U. Formation of highly oxygenated organic molecules from aromatic compounds. Atmospheric Chemistry and Physics, **18** (3), 1909, **2018**.
54. DONG Z.K., TANG R.Y., LIU H.F., ZHANG Q.Z., ZONG W.S., CHENG J.M., SHI X.L. The formation mechanism of highly oxygenated organic molecules produced by toluene in the urban atmosphere. Atmospheric Environment, **295**, 119555, **2023**.
55. ALTIERI K.E., SEITZINGER S.P., CARLTON A.G., TURPIN B.J., KLEIN G.C., MARSHALL A.G. Oligomers formed through in-cloud methylglyoxal reactions: Chemical composition, properties, and mechanisms investigated by ultra-high resolution FT-ICR mass spectrometry. Atmospheric Environment, **42** (7), 1476, **2023**.
56. MARKOVIĆ S., TOŠOVIĆ J. Application of time-dependent density functional and natural bond orbital theories to the UV–vis absorption spectra of some phenolic compounds. The Journal of Physical Chemistry A, **119** (35), 9352, **2015**.
57. SATO K., TAKAMI A., ISOZAKI T., HIKIDA T., SHIMONO A., IMAMURA T. Mass spectrometric study of secondary organic aerosol formed from the photo-oxidation of aromatic hydrocarbons. Atmospheric Environment, **44** (8), 1080, **2010**.

Supplementary Information

Link to the file https://www.pjoes.com/SuppFile/224835/1/